Volume 17
Number 26
14 July 2025
Pages 15539-16042

Nanoscale

rsc.li/nanoscale

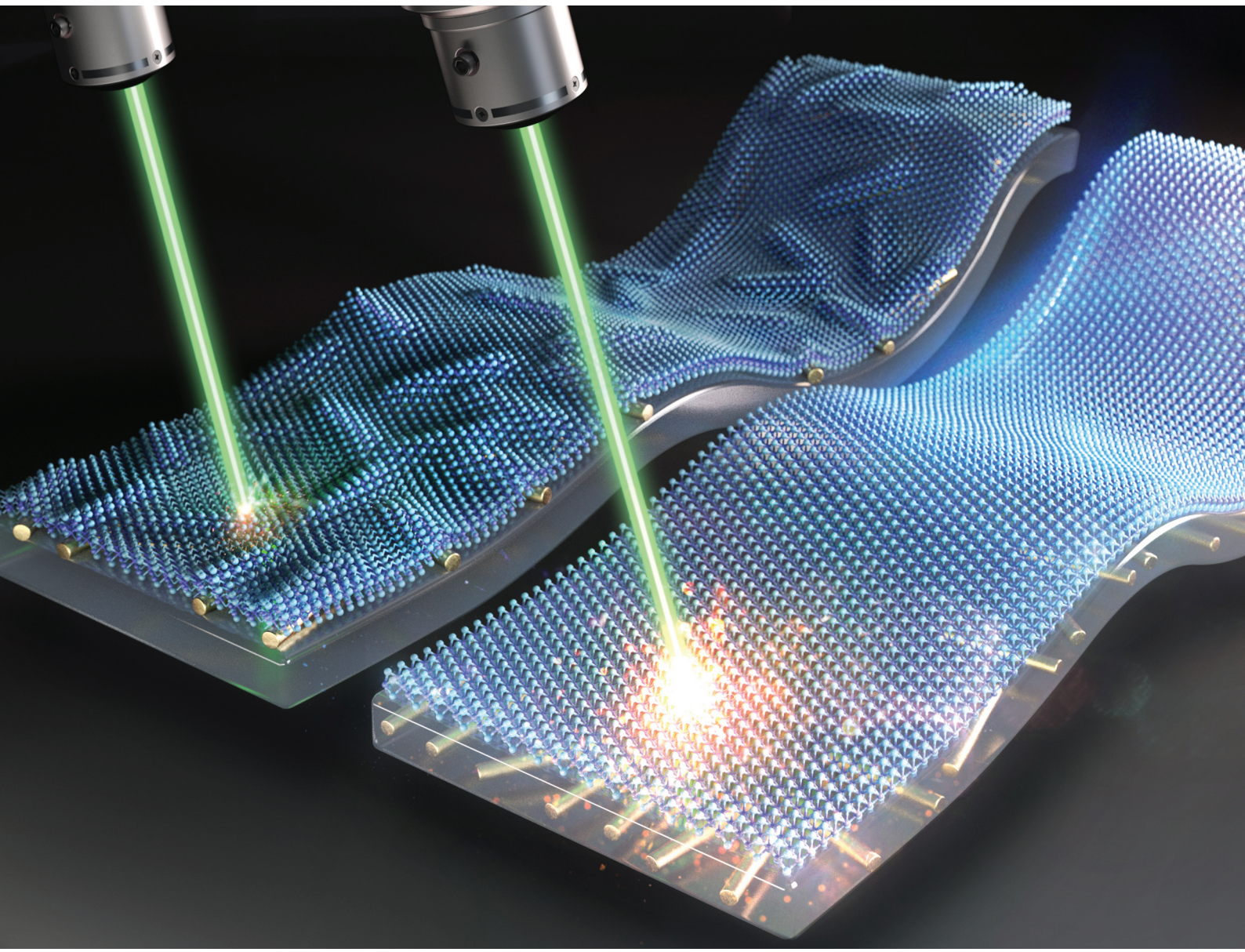

ISSN 2040-3372

ROYAL SOCIETY OF CHEMISTRY

COMMUNICATION

Dong-Wook Kim *et al.*

Optimized plasmonic enhancement and deformation reduction in MoS_2 monolayers using Au-nanowire-embedded polymers

NCNST

Nanoscale

ROYAL SOCIETY OF CHEMISTRY

COMMUNICATION

View Article Online
View Journal | View Issue

Open Access Article. Published on 14 May 2025. Downloaded on 1/21/2026 7:28:19 AM.
This article is licensed under a Creative Commons Attribution-NonCommercial 3.0 Unported Licence.

Check for updates

Cite this: *Nanoscale*, 2025, **17**, 15690

Received 19th March 2025,
Accepted 14th May 2025

DOI: 10.1039/d5nr01147g

rsc.li/nanoscale

Optimized plasmonic enhancement and deformation reduction in MoS_2 monolayers using Au-nanowire-embedded polymers†

Nahyun Kim,[a] Jungeun Song,[a] Jungyoon Cho,[a] Anh Thi Nguyen,[a] Seawoo Moon,[a] Ambrose Seo [a,b] and Dong-Wook Kim *[a]

Hybrid systems consisting of transition metal dichalcogenide (TMD) layers and metal nanostructures offer promising opportunities to control excitonic behaviors and enhance light–matter interaction in TMDs. This work introduces an unprecedented approach to integrate exfoliated MoS_2 monolayers with gold nanowire (AuNW)-embedded PDMS films. Localized surface plasmon excitation in AuNWs boosts light scattering, as evidenced by optical characterization and numerical simulations. Notably, MoS_2 monolayers on AuNW-embedded PDMS films exhibit a five-fold increase in photoluminescence intensity compared to those on non-embedded AuNW/PDMS substrates. This enhancement arises from the extended and intensified electric fields resulting from the substantial dielectric permittivity contrast between PDMS and air. Furthermore, embedding AuNWs effectively mitigates mechanical deformation of MoS_2 monolayers, suppressing strain-induced dissociation of photo-generated excitons. These findings demonstrate the potential of AuNW-embedded polymers for advanced TMD-based plasmonic device applications.

1. Introduction

Two-dimensional (2D) semiconductor materials, particularly transition metal dichalcogenides (TMDs), provide a promising platform for exploring intriguing physical phenomena due to their quantum confinement effects and an exceptionally high surface-to-volume ratio.[1–13] Monolayer (1L) TMDs exhibit sizable direct bandgaps and extraordinarily large exciton binding energies, enabling highly efficient optical absorption and emission.[2–6] However, their atomic-scale physical thickness limits light–matter interactions,[3,4] necessitating innovative strategies to optimize their performance in optoelectronic device applications.

To address these challenges, TMDs can be integrated with metal nanostructures, which amplify local electromagnetic fields through plasmonic effects.[7–13] Typically, two approaches are employed for this integration: (i) preparing metal nanostructures on the TMD surface[7,8] and (ii) transferring TMD layers onto prefabricated metal nanostructures.[8–13] However, each approach presents its own limitations. Metal nanostructures on TMD surfaces can hinder light absorption in TMD layers due to their large scattering cross-sections, while transferring TMD layers onto metal nanostructures often leads to local mechanical deformation of the ultrathin TMD layers caused by the non-flat surface of the underlying nanostructures.[9,10] Inhomogeneous strain distributions can effectively funnel photogenerated excitons toward higher-strained regions, which can be beneficial for single photon sources and solar cells.[4] However, the spatial separation of excitons can impede their radiative recombination.[11] Therefore, a strategy to independently tune mechanical strain and plasmonic effects is required to optimize the desirable characteristics of TMD-metal integrated systems.

Gold nanowires (AuNWs) are widely recognized as plasmonic nanostructures due to their excellent characteristics in the visible wavelength range.[14–16] Among various metal nanostructures, such as nanoparticles and nanogrooves, AuNWs offer several distinct advantages for TMD-metal integration. The plasmonic properties of AuNWs can be tuned by modifying their geometric parameters, such as length and diameter, as well as by altering the surrounding dielectric environment.[12–16] The anisotropic geometry of metal nanowires induces polarization-dependent optical responses, enabling clear identification of surface plasmon excitation.[14–16] Additionally, their elongated geometry of AuNWs generates an extended electromagnetic field along the wire axis, facilitating more uniform and spatially extended light–matter interaction with TMDs.[14–16]

A major technical challenge is the efficient integration of AuNWs with TMD layers. Conventional tape-based mechanical exfoliation techniques usually produce TMD flakes that are

[a]*Department of Physics, Ewha Womans University, Seoul 03760, Korea. E-mail: dwkim@ewha.ac.kr*
[b]*Department of Physics and Astronomy, University of Kentucky, Lexington, Kentucky 40506, USA*

†Electronic supplementary information (ESI) available: Optical microscope images of Au nanowires; sample fabrication processes; atomic force microscope images and profiles; polarization-dependent photoluminescence spectra. See DOI: https://doi.org/10.1039/d5nr01147g

This journal is © The Royal Society of Chemistry 2025

Open Access Article. Published on 14 May 2025. Downloaded on 1/21/2026 7:28:19 AM.
This article is licensed under a Creative Commons Attribution-NonCommercial 3.0 Unported Licence.

only several microns in size,[2–5] making it difficult to stack them with AuNWs of similar dimensions. Moreover, transfer techniques often suffer from low yield, and conducting comparative studies on identical flake regions with and without AuNWs becomes practically impossible. To overcome these issues, metal-assisted atomic spalling has been adopted as an alternative exfoliation method.[17] This technique leverages strong van der Waals or covalent-like quasi-bonding interactions between metals and TMD layers, enabling the production of large-area 1L TMD flakes extending up to a few hundreds of micrometers.

In this work, two types of TMD-metal integrated structures are fabricated using large-area 1L-MoS_2 flakes integrated with AuNWs. Polydimethylsiloxane (PDMS) polymer films are employed as substrates to mitigate strain effects induced by AuNWs. In the first configuration, AuNWs are simply rested on the surface of PDMS films, followed by the transfer of exfoliated 1L-MoS_2 flakes onto these films. In the second configuration, AuNWs are embedded within the PDMS films, and exfoliated 1L-MoS_2 flakes are subsequently transferred onto the AuNW-embedded films. Comprehensive optical characterizations and numerical simulations reveal that embedding AuNWs within the PDMS films do not only reduce mechanical deformation but also enhance plasmonic benefits in the MoS_2 monolayers. These results highlight the benefits of AuNW-embedded substrates as a viable strategy for optimizing plasmonic effects in TMD-based optoelectronic devices.

2. Experimental

Raman scattering and photoluminescence (PL) measurements were conducted using a microscope-based system (XperRAM, Nanobase). A 532 nm-laser (Cobolt 08-DPL, Cobolt) was used as the excitation source, with an optical power of 0.2 mW to prevent sample damage. The laser beam was focused through a 40× objective lens with a numerical aperture of 0.75 (MplanFLN, Olympus). Data acquisition times were set to 0.5 s for PL measurements and 5 s for Raman measurements to improve the signal-to-noise ratio. Both PL and Raman measurements were conducted in ambient air and at room temperature.

Numerical simulations were performed using commercial finite-difference time-domain (FDTD) software (Lumerical Solutions, Ansys) to obtain the electric field distributions in the samples under illumination. In all simulations, a plane wave light source was normally incident on the sample surface, and the visible wavelength range (400–800 nm) was considered. A mesh size of $2.0 \times 2.0 \times 2.0$ nm^3 was used for the calculations. For the FDTD simulations, perfectly matched layer (PML) boundary conditions were applied in the out-of-plane direction, whereas symmetric and anti-symmetric boundary conditions were employed in the in-plane directions. The optical constants of PDMS and Au were taken from the literature.[17,18]

3. Results

MoS_2 flakes were prepared using the metal-assisted atomic spalling technique, following the procedures reported in ref. 18. The 1L regions of the exfoliated MoS_2 flakes were much larger than AuNWs (purchased from Nanopartz) with an average length of about 5 μm (Fig. S1, ESI†). As shown in Fig. 1(a) and (b), MoS_2 flakes were integrated with two types of AuNW-containing PDMS films: (i) AuNWs placed on the PDMS surface and (ii) AuNWs embedded within the PDMS film. For simplicity, these distinct configurations are denoted as M/NW (ON) and M/NW(IN) hereafter. Detailed fabrication processes for the AuNW-containing PDMS films, M/NW(ON) and M/NW (IN) are provided in Fig. S1 and S2 (ESI†). In the optical microscope (OM) images (Fig. S2(b) and (c), ESI†), the bright AuNWs are clearly visible, and the optical contrast of the MoS_2 flakes varies according to their thickness. The surface topography of the samples was characterized using an atomic force microscopy (AFM) system (NX-10, Park Systems).

Fig. 1(a) and (b) show the polarization-dependent OM images of M/NW(ON) and M/NW(IN), respectively. In each figure, the left images correspond to transverse illumination, where the electric field is perpendicular to the AuNW axis, and the right images correspond to longitudinal illumination, with the electric field parallel to the AuNW axis. Under both illumination conditions, the 1L MoS_2 regions on AuNWs appear brighter than the surrounding regions without AuNWs even though the AuNW diameter is only 50 nm – significantly smaller than the wavelength of visible light. Notably, AuNWs exhibit higher optical contrast under transverse illumination compared to longitudinal illumination. This distinct contrast arises from the localized surface plasmon (LSP) excitation in AuNWs, which enhances light scattering.[14–16] For 50 nm-diameter AuNWs, transverse LSP resonances occur near λ = 520 nm,[14,19] resulting in a large optical cross-section at short visible wavelengths (Fig. S3, ESI†). In contrast, the longitudinal LSP resonance for micron-length AuNWs occurs in the near infrared range.[14] Consequently, transverse LSP excitation in AuNWs contributes to the pronounced contrast observed in the OM images obtained using visible-light LEDs.

The AFM height profiles obtained from M/NW(ON) and M/NW(IN) are shown in Fig. 1(c) and (d), respectively. For M/NW (ON), the AFM profile in Fig. 1(c) indicates a height of approximately 50 nm in the 1L region on AuNW, which is consistent with the average diameter of AuNWs (Fig. S4(a), ESI†). In contrast, the AFM images for M/NW(IN) (Fig. 1(d)) reveal a height of only about 10 nm in the 1L region on AuNW. During the degassing and curing processes, the PDMS mixture may not be completely wrapped around AuNWs in M/NW(IN), leaving parts of their surfaces exposed to air (Fig. S4(b), ESI†). As a result, portions of the embedded AuNWs in M/NW(IN) protrude from the PDMS surface, as illustrated in Fig. 1(d).

Fig. 2(a) and (b) show the polarization-dependent PL spectra of 1L MoS_2 regions with and without AuNWs in M/NW (ON) and M/NW(IN), respectively. The labels "T" and "L" denote the transverse and longitudinal illumination con-

Open Access Article. Published on 14 May 2025. Downloaded on 1/21/2026 7:28:19 AM.
This article is licensed under a Creative Commons Attribution-NonCommercial 3.0 Unported Licence.

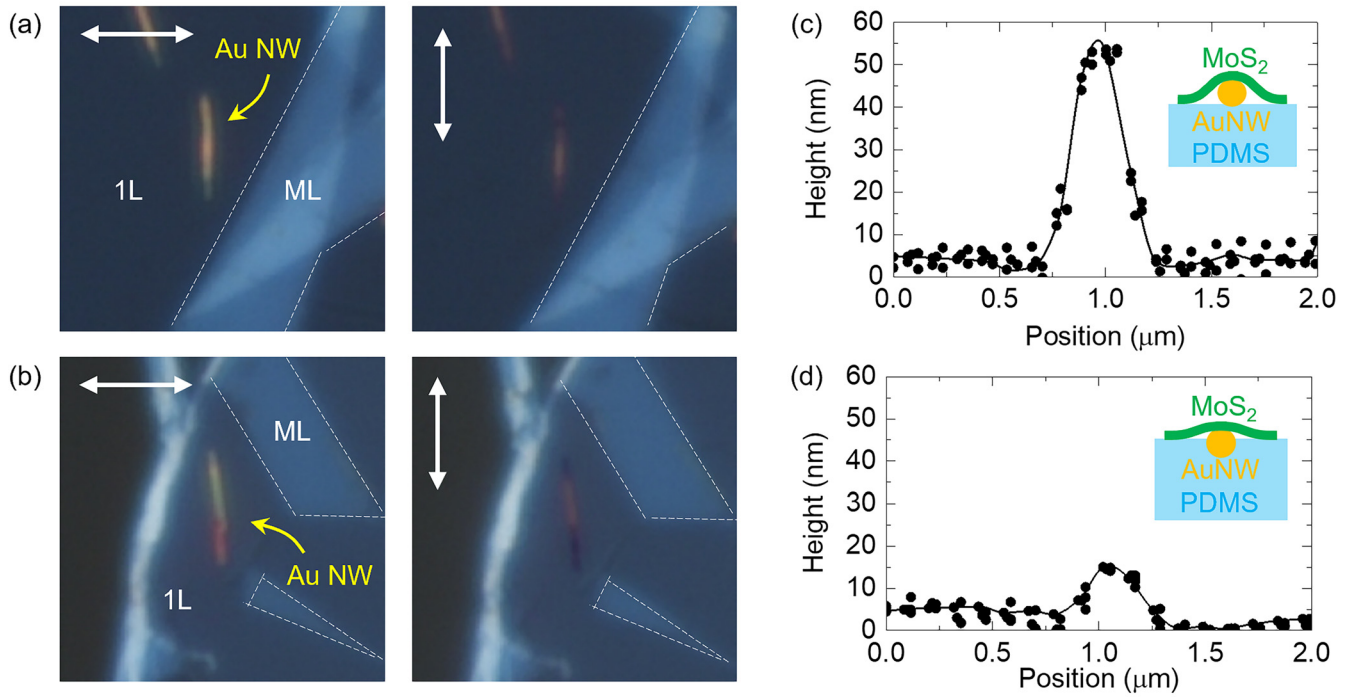

Fig. 1 Polarization-dependent OM images (size: 15 μm × 15 μm) of (a) M/NW(ON) and (b) M/NW(IN), with labelled 1L MoS_2 regions, multilayer (ML) MoS_2 regions, PDMS surfaces, and AuNWs. While arrows indicate the light polarization directions. Height profiles and cross-sectional schematic diagrams of (c) M/NW(ON) and (d) M/NW(IN). In the profiles, symbols represent raw data acquired from multiple line scans across AuNWs and lines indicate their average values.

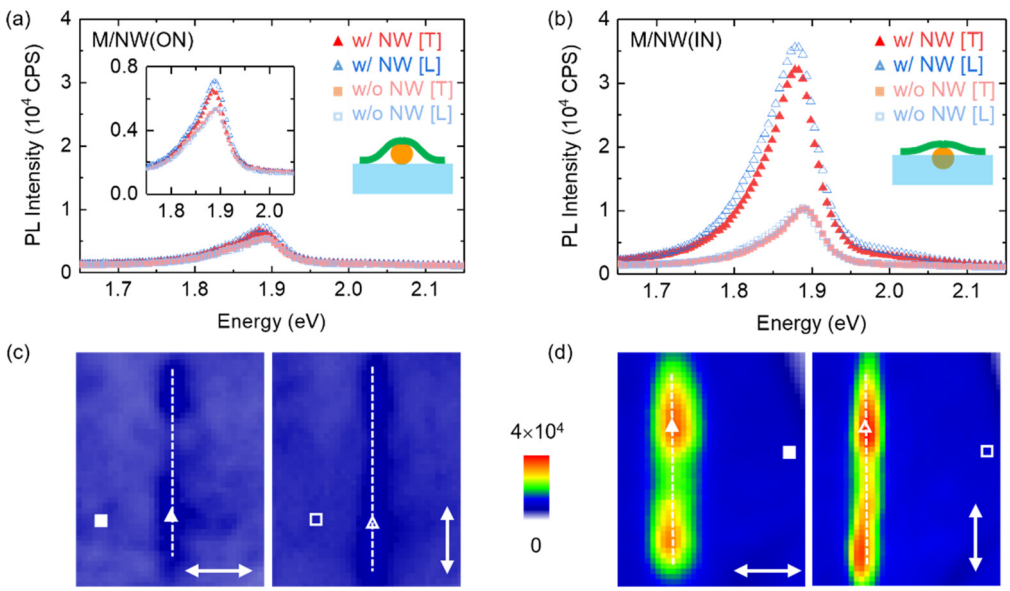

Fig. 2 Polarization-dependent (a and b) PL spectra and (c and d) PL intensity maps (area: 4 μm × 5 μm) of M/NW(ON) and M/NW(IN). In (a) and (b), T and L denote transverse and longitudinal illumination conditions, respectively, with spectra compared for regions with AuNWs (w/NW) and without AuNWs (w/o NW). The inset in (a) with expanded *y*-axis scale clearly compares the PL intensities of M/NW(ON). While arrows in (c) and (d) indicate the light polarization directions.

ditions. The dominant PL peaks, observed near 1.9 eV, are consistent with previously reported spectra of 1L MoS_2 flakes.[2–5,9,11] For M/NW(ON), the presence of AuNWs results in a slight increase in PL intensity (Fig. 2(a)), which is further visualized in the PL intensity map (Fig. 2(c)). In contrast, the PL spectra for M/NW(IN) (Fig. 2(b)) exhibit a significant

 This journal is © The Royal Society of Chemistry 2025

Open Access Article. Published on 14 May 2025. Downloaded on 1/21/2026 7:28:19 AM.
This article is licensed under a Creative Commons Attribution-NonCommercial 3.0 Unported Licence.

increase in the PL intensity in MoS_2 regions containing AuNWs. The corresponding PL intensity map (Fig. 2(d)) confirms this observation, indicating stronger PL signals in AuNW-containing regions compared to the surrounding regions. Quantitatively, the AuNW-induced PL enhancement ratio for M/NW(IN) reaches 300%, markedly exceeding the 120% enhancement observed for M/NW(ON). Furthermore, the PL intensity of the AuNW-containing region in M/NW(IN) is nearly 5 times larger than that in M/NW(ON).

The pronounced optical contrast in the OM images (Fig. 1(a) and (b)) suggests that LSP-induced light scattering from AuNWs boosts optical absorption in the 1L MoS_2 regions on top of AuNWs, thereby increasing the PL intensities. However, for M/NW(ON), the topographic modulation of the 1L MoS_2 regions on AuNWs (Fig. 1(c)) induces mechanical strain, leading to band gap modulation in the strained MoS_2 regions.[4,11] Non-uniform strain distributions in MoS_2 layers can lead to exciton dissociation and suppress the radiative recombination of photo-generated excitons, thereby limiting PL enhancement.[11] Conversely, the reduced topographic modulation in M/NW(IN) minimizes strain in the 1L MoS_2 regions on AuNWs (Fig. 1(d)), resulting in a more pronounced AuNW-induced PL enhancement compared to M/NW(ON).

As shown in Fig. 2(a) and (b), the PL peaks in AuNW-containing regions exhibit a redshift in both M/NW(ON) and M/NW(IN). This redshift is attributed to LSP-induced local heating *via* two routes; (1) enhanced absorption due to strong scattering from AuNWs, leading to a temperature increase in MoS_2, and (2) heat transfer from AuNWs to adjacent MoS_2 regions.[9] Elevated temperatures reduce the bandgap of MoS_2, resulting in a redshift of PL peaks.[9,20] Quantitative analyses of the PL subpeaks in M/NW(ON) reveal a redshift of ~5 meV in the A exciton peak within AuNW-containing region compared to AuNW-free region under transverse illumination (Fig. S5(a), ESI†). In M/NW(IN), this redshift is more pronounced, reaching ~11 meV under transverse illumination (Fig. S5(b), ESI†). Using the peak shift coefficient reported by Plechinger *et al.*,[20] the temperature difference between AuNW-containing and AuNW-free regions (ΔT-AuNW) is estimated to be around 15 K for M/NW(ON) and 40 K for M/NW(IN). Additionally, thermal effects can induce biaxial tensile strain in MoS_2 flakes on PDMS films due to the large difference in their thermal expansion coefficients,[20] leading to further band gap modulation and a red shift in the PL peaks. The greater AuNW-induced PL enhancement (Fig. 2(a) and (b)) and the larger ΔT-AuNW suggests that the plasmonic effects of AuNWs more significantly influence the optical characteristics of 1L MoS_2 flakes in M/NW(IN).

Several mechanisms can be considered to explain the PL characteristics of semiconductor–metal nanostructures: (1) LSP-mediated scattering enhances emission, while LSP-induced absorption suppresses it; (2) local field enhancement increases both the excitation rate and the radiative recombination rate;[3,9] (3) the electron transfer from metals to semiconductors can enhance PL, whereas the electron transfer from semiconductors to metals results in PL quenching;[3,8] and (4) LSP-induced heating suppresses radiative recombination processes.[9] Since the enhancement and quenching processes compete, LSP excitation does not always lead to increased PL intensity of hybrid systems. The PL intensity under transverse illumination decreases by 7% for M/NW(ON) and 10% for M/NW(IN) compared to longitudinal illumination (Fig. 2(a) and (b)). Under 532 nm excitation, the transverse LSP excitation can increase absorption in AuNWs, leading to a reduction in the PL intensity. The trion-to-exciton ratio does not increase under transverse illumination compared to longitudinal illumination (Fig. S5(a) and (b), ESI†), suggesting an absence of direct evidence for LSP-induced electron transfer from AuNWs to MoS_2. Elevated temperatures enhance the thermal motion of phonons, which in turn promotes non-radiative recombination processes, thereby diminishing PL intensity.[21,22] A temperature rise of 30 K (from 270 to 300 K) can lead to a twofold decrease in PL intensity in 1L MoS_2.[21] Therefore, the observed PL enhancement in our samples overcomes thermal quenching, underscoring the dominant contribution of plasmonic effects.

Although our samples were prepared in humidity-controlled environments (<30% RH) and stored in vacuum to minimize water adsorption, an interfacial water layer between MoS_2 and AuNW might be present and can work as a barrier to charge transfer.[13,23] However, any residual water layer is likely comparable between M/NW(ON) and M/NW(IN), and thus cannot account for the distinct PL behavior. In addition, dielectric screening effects should be considered. For MoS_2 partially suspended in air (M/NW(ON)), a reduced effective dielectric constant should increase exciton binding energy and lead to a redshifted PL peak. The experimental results show the opposite trend—M/NW(IN) exhibits a lower energy PL peak. This suggests that dielectric screening alone cannot explain the results.[24,25] To further examine the influence of excitation power, PL measurements at reduced power (0.02 mW) were also carried out (Fig. S6, ESI†). No noticeable peak shifts were observed in AuNW-containing regions under low power, in contrast to the pronounced red shifts at 0.2 mW (Fig. 2(a) and (b)). These results confirm that the observed redshift at higher power originates from local heating near AuNWs.

Fig. 3(a) and (b) show the polarization-dependent Raman spectra of 1L MoS_2 regions with and without AuNWs in M/NW (ON) and M/NW(IN), respectively. In AuNW-free regions, the characteristic peaks of 1L MoS_2 appear near 382 cm^{-1} and 402 cm^{-1}, corresponding to the in-plane E′ and out-of-plane A_1' vibrational modes, respectively. The peak spacing of ~20 cm^{-1} between E′ and A_1' confirms the successful preparation of 1L MoS_2 flakes.[4,5]

Slight variations in peak positions and intensities between AuNW-free regions in M/NW(ON) and M/NW(IN) (Table 1) are likely due to distinct strain states in the MoS_2 flakes through different sample fabrication processes.[26–28] In both M/NW(ON) and M/NW(IN), the presence of AuNWs increases the Raman intensity of the 1L regions, with a more pronounced enhancement observed in M/NW(IN). The substantial increase in the characteristic peaks in AuNW-containing regions compared to

Open Access Article. Published on 14 May 2025. Downloaded on 1/21/2026 7:28:19 AM.
This article is licensed under a Creative Commons Attribution-NonCommercial 3.0 Unported Licence.

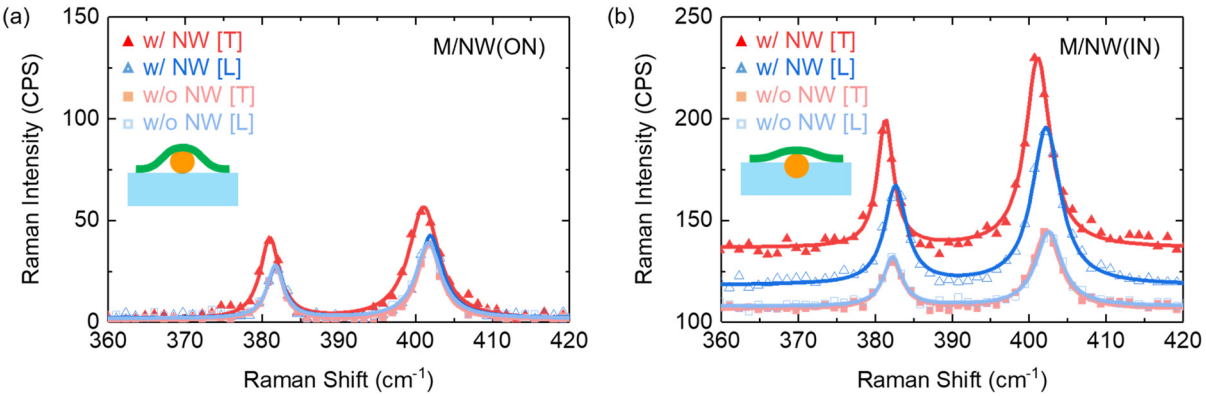

Fig. 3 Raman spectra of (a) M/NW(ON) and (b) M/NW(IN). T and L denote transverse and longitudinal illumination conditions, respectively, with spectra compared for regions with AuNWs (w/NW) and without AuNWs (w/o NW).

Table 1 Polarization-dependent E′ and A_1' peaks of with AuNWs (w/NW) and without AuNWs (w/o NW) in M/NW(ON) and M/NW(IN)

M/NW(ON)	Peak (cm^{-1})		M/NW(IN)	Peak (cm^{-1})	
w/NW [T]	E′	381.0	w/NW [T]	E′	381.3
	A_1'	401.0		A_1'	401.1
w/NW [L]	E′	381.8	w/NW [L]	E′	382.5
	A_1'	401.9		A_1'	402.2
w/o NW [T]	E′	381.7	w/o NW [T]	E′	382.2
	A_1'	401.7		A_1'	402.2
w/o NW [L]	E′	381.7	w/o NW [L]	E′	382.2
	A_1'	401.6		A_1'	402.5

T and L denote transverse and longitudinal illumination conditions, respectively.

AuNW-free regions suggests a strong LSP effect. As discussed earlier, the transverse LSP resonance occurs near 530 nm (the excitation wavelength used for both PL and Raman measurements), resulting in an amplified local electromagnetic field near AuNWs. The strong PL background emission from 1L MoS_2, as evident in Fig. 2(b), raises the baseline of the Raman spectra and obscures quantitative comparison of the peak intensity changes, particularly in M/NW(IN). PL and Raman signals originate from distinct physical processes: PL arises from radiative recombination of excitons generated by absorbed photons, whereas Raman scattering is an inelastic process involving phonon interactions. Therefore, differences between M/NW(ON) and M/NW(IN) cannot be solely attributed to variations in optical absorption.

In both M/NW(ON) and M/NW(IN), the Raman spectra from AuNW-containing regions exhibit polarization dependence, with peak intensity variations and peak shifts. Under transverse illumination, the AuNW-induced peak shifts for the E′ and A_1' modes in M/NW(ON) are -0.7 cm^{-1} and -0.7 cm^{-1}, respectively, while in M/NW(IN), the corresponding shifts are -0.9 cm^{-1} and -1.1 cm^{-1}, as summarized in Table 1. In contrast, under longitudinal illumination, the AuNW-induced peak shifts are small: $+0.1$ cm^{-1} (E′) and $+0.3$ cm^{-1} (A_1') for M/NW(ON), and $+0.3$ cm^{-1} (E′) and -0.3 cm^{-1} (A_1') for M/NW(IN). The E′ and A_1' peak positions are known to be sensitive to strain and carrier concentration, respectively.[27–29] The observed peak shifts under specific polarization conditions cannot be solely explained by strain of carrier concentration changes. Instead, they likely result from local heating near AuNWs induced by LSP excitation. It has been reported that local heating on MoS_2 leads to a redshift in both E′ and A_1' peaks.[26] The temperature difference between AuNW-containing and AuNW-free regions, ΔT-AuNW, under transverse illumination can be estimated using the peak shift coefficients reported by Yang *et al.*[26] The estimated ΔT-AuNW for M/NW(IN) is higher than that for M/NW(ON) by approximately 20–40 K, which is comparable to the ΔT-AuNW value derived from the PL peak shift.

Fig. 4(a) and (b) show the FDTD-simulated electric field intensity distributions for AuNWs placed on the surface of a PDMS film and embedded within a PDMS film, respectively, under transverse illumination at a wavelength of 530 nm. In both AuNW-on-PDMS and AuNW-embedded-PDMS, a strongly concentrated electric field appears near AuNWs. For comparison, the electric field intensities around AuNWs are decomposed into their in-plane ($|E_x|^2$) and out-of-plane ($|E_z|^2$) components. Since the electric field of the incident light is parallel to E_x, the oscillatory motion of free electrons in AuNWs induces strong electric dipoles along the in-plane direction. Consequently, the total electric field intensity, $|E|^2$, is dominantly determined by $|E_x|^2$ in both AuNW-on-PDMS and AuNW-embedded-PDMS. Moreover, $|E_x|^2$ exhibits its maximum value at the lateral surface of AuNWs, while its minimum at the top and bottom surfaces of AuNWs. Notably, the maximum $|E_x|^2$ at the AuNW surface exceeds the minimum by two orders of magnitude, indicating significant spatial variation in $|E_x|^2$ depending on the position.

When MoS_2 flakes are illuminated, the electric field components of the incident light that are parallel to the flake surface effectively contribute to optical absorption, whereas the perpendicular components do not, due to the extremely small physical thickness of MoS_2.[29] In M/NW(ON), the MoS_2 flake surface (with presumed contours denoted by dashed gray

 This journal is © The Royal Society of Chemistry 2025

Open Access Article. Published on 14 May 2025. Downloaded on 1/21/2026 7:28:19 AM.
This article is licensed under a Creative Commons Attribution-NonCommercial 3.0 Unported Licence.

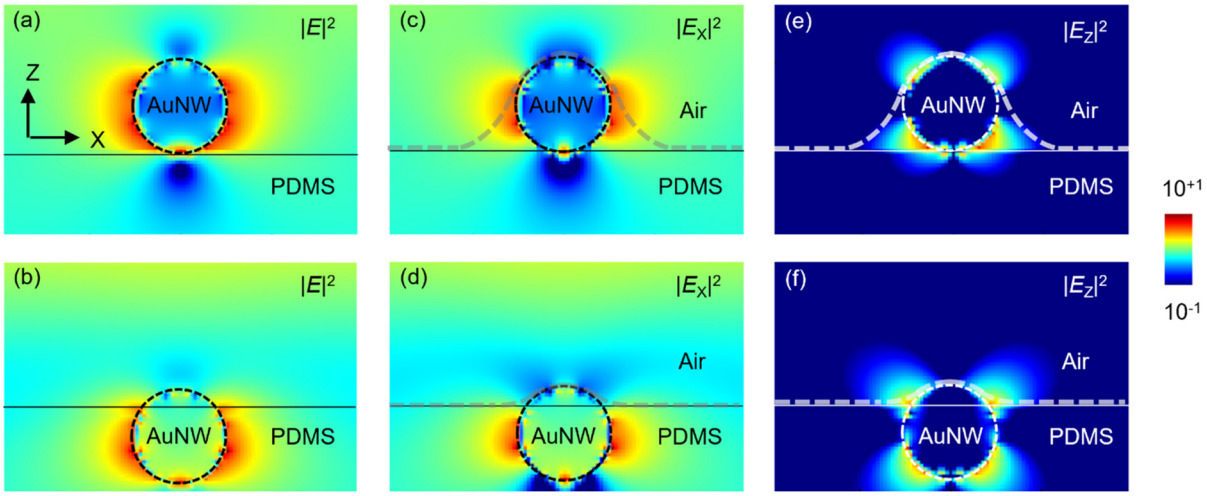

Fig. 4 FDTD-calculated electric field (E) intensity distributions for (a) M/NW(ON) and (b) M/NW(IN) at wavelength of 530 nm. The intensities of the (c and d) in-plane (E_x) and (e and f) out-of-plane (E_z) components of M/NW(ON) and M/NW(IN) are compared.

lines in Fig. 4(a)) is inclined relative to the x-axis near the lateral surface of AuNWs, where a strong E_x field is present. However, at the top surface of AuNWs, the flake surface becomes parallel to the x-axis, where the E_x component is weak (Fig. 4(a)). In contrast, in M/NW(IN), a relatively large E_x is observed across the entire flake surface. These findings suggest that the effective region, where the plasmonic effects of AuNWs enhance optical absorption in MoS_2, is significantly more restricted in M/NW(ON) compared to M/NW(IN). The extended and intensified electric field leads to the more pronounced increase in PL and Raman intensities observed in M/NW(IN) (Fig. 2(a, b) and 3(a, b)). The distinct field distributions also explain the reason why more extended PL enhancement regions appear for M/NW(IN), as shown in Fig. 2(c) and (d).

4. Conclusions

Two types of TMD-metal integrated structures, MoS_2/AuNW-on-PDMS (M/NW(ON)) and MoS_2/AuNW-embedded-PDMS (M/NW(IN)), were fabricated using a metal-assisted atomic spalling method followed by a dry transfer process. The polarization-dependent optical contrast of AuNWs indicated transverse LSP excitation in the visible wavelength range. Comparative characterizations of the two configurations revealed that M/NW(IN) exhibited five-fold enhanced PL intensities compared to M/NW(ON), which can be attributed to the embedded AuNWs effectively reducing mechanical deformation and mitigating strain-induced exciton dissociation. FDTD simulations supported these results, demonstrating that M/NW(IN) generated a stronger in-plane electric field component over the MoS_2 flakes than M/NW(IN). The strategy of embedding AuNWs into polymer substrates provides a versatile route to decouple mechanical effects from plasmonic enhancement in TMD-Au integrated nanostructures.

Author contributions

Nahyun Kim: conceptualization, investigation, data curation, writing – original draft, writing – review and editing. Jungeun Song: conceptualization, investigation, data curation. Jungyoon Cho, Anh Thi Nguyen, Seawoo Moon, Seoyoung Lim: investigation, data curation. Ambrose Seo: investigation, writing – review and editing. Dong-Wook Kim: conceptualization, writing – original draft, writing – review and editing, supervision.

Data availability

The data that support the findings of this study are available from the corresponding author upon reasonable request.

Conflicts of interest

There are no conflicts to declare.

Acknowledgements

This work was supported by the National Research Foundation of Korea (NRF) grants funded by the Korea Government (RS-2024-00341837, RS-2024-00391757, and RS-2024-00406827).

References

1 K. S. Kim, J. Kwon, H. Ryu, C. Kim, H. Kim, E.-K. Lee, D. Lee, S. Seo, N. M. Han, J. M. Suh, J. Kim, M.-K. Song, S. Lee, M. Seol and J. Kim, *Nat. Nanotechnol.*, 2024, **19**, 895.

Open Access Article. Published on 14 May 2025. Downloaded on 1/21/2026 7:28:19 AM.
This article is licensed under a Creative Commons Attribution-NonCommercial 3.0 Unported Licence.

2 L. Huang, A. Krasnok, A. Alu, Y. Yu, D. Neshev and A. E. Miroshnichenko, *Rep. Prog. Phys.*, 2022, **85**, 046401.
3 A. J. Moilanen, M. Cavigelli, T. Taniguchi, K. Watanabe and L. Novotny, *ACS Nano*, 2025, **19**, 4731.
4 Z. Peng, X. Chen, Y. Fan, D. J. Srolovitz and D. Lei, *Light: Sci. Appl.*, 2020, **9**, 190.
5 K. M. McCreary, A. T. Hanbicki, S. V. Sivaram and B. T. Jonker, *APL Mater.*, 2018, **6**, 111106.
6 H. Wang, W. Wang, Y. Zhong, D. Li, Z. Li, X. Xu, X. Song, Y. Chen, P. Huang, A. Mei, H. Han, T. Zhai and X. Zhou, *Adv. Mater.*, 2022, **34**, 2206122.
7 J. Shi, J. Zhu, X. Wu, B. Zheng, J. Chen, X. Sui, S. Zhang, J. Shi, W. Du, Y. Zhong, Q. Wang, Q. Zhang, A. Pan and X. Liu, *Adv. Opt. Mater.*, 2020, **8**, 2001147.
8 P. Sriram, A. Manikandan, F.-C. Chuang and Y.-L. Chueh, *Small*, 2020, **16**, 1904271.
9 S. Najmaei, A. Mlayah, A. Arbouet, C. Girard, J. Léotin and J. Lou, *ACS Nano*, 2014, **8**, 12682.
10 B. N. Tugchin, N. Doolaard, A. I. Barreda, Z. Zhang, A. Romashkina, S. Fasold, I. Staude, F. Eilenberger and T. Pertsch, *Nano Lett.*, 2023, **23**, 10848.
11 J. Song, S. Kwon, B. Kim, E. Kim, L. N. S. Murthy, T. Lee, I. Hong, B. H. Lee, S. W. Lee, S. H. Choi, K. K. Kim, C. H. Cho, J. W. P. Hsu and D.-W. Kim, *ACS Appl. Mater. Interfaces*, 2020, **12**, 48991.
12 C. Han, Y. Wang, W. Zhou, M. Liang and J. Ye, *Sci. Rep.*, 2021, **11**, 10080.
13 H. Chen, J. Yang, E. Rusak, J. Straubel, R. Guo, Y. W. Myint, J. Pei, M. Decker, I. Staude, C. Rockstuhl, Y. Lu, Y. S. Kivshar and D. Nershev, *Sci. Rep.*, 2016, **6**, 22296.
14 Y.-F. Chau, M. W. Chen and D. P. Tsai, *Appl. Opt.*, 2009, **48**, 617.
15 A. S. Lal, J. H. Hafner, N. J. Halas, S. Link and P. Nordlander, *Acc. Chem. Res.*, 2012, **45**, 1887–1895.
16 P. Bell, J. A. Fairfield, E. K. McCarthy, S. Mills, J. J. Boland, G. Baffou and D. McCloskey, *ACS Nano*, 2015, **9**, 5551–5558.
17 E. D. Palik, *Handbook of Optical Constants of Solids*, Academic Press, 1985.
18 D. R. Lide, *CRC Hand Book of Chemistry and Physics*, CRC Press, 76th edn, 1995.
19 A. Mooradian, *Phys. Rev. Lett.*, 1969, **22**, 185.
20 G. Plechinger, A. Castellanos-Gomez, M. Buscema, H. S. J. van der Zant, G. A. Steele, A. Kuc, T. Heine, C. Schüller and T. Korn, *2D Mater.*, 2015, **2**, 015006.
21 H. Li and X. H. Zhang, *Opt. Mater.*, 2020, **107**, 110150.
22 S. Golovynskyi, I. Irfan, M. Bosi, L. Seravalli, O. I. Datsenko, I. Golovynska, B. Li, D. Lin and J. Qu, *Appl. Surf. Sci.*, 2020, **515**, 146033.
23 R. J. P. Román, Y. Auad, L. Crasso, F. Alvarez, I. D. Barcelos and L. F. Zagonel, *Nanoscale*, 2020, **12**, 13460.
24 Y. Lin, X. Ling, L. Yu, S. Huang, A. L. Hsu, Y.-H. Lee, J. Kong, M. S. Dresslhaus and T. Palacios, *Nano Lett.*, 2014, **14**, 5569.
25 L. Wang, Z. N. Nilsson, M. Tahir and J. B. Sambur, *ACS Appl. Mater. Interfaces*, 2020, **12**, 15034.
26 Y. Yang, Z. T. Lin, R. F. Lin, Y. T. Li, W. G. Liu, S. B. Tian, K. Zhu and L. C. Long, *Microstructures*, 2021, **1**, 2021002.
27 J.-U. Lee, K. Kim and H. Cheong, *2D Mater.*, 2015, **2**, 044003.
28 B. Chakraborty, A. Bera, D. V. S. Muthu, S. Bhowmick, U. V. Waghmare and A. K. Sood, *Phys. Rev. B:Condens. Matter Mater. Phys.*, 2012, **85**, 161403(R).
29 K. M. Islam, R. Synowicki, T. Ismael, I. Oguntoye, N. Grinalds and M. D. Escarra, *Adv. Photonics Res.*, 2021, **2**, 2000180.

This journal is © The Royal Society of Chemistry 2025